BİNGÖL UNIVERSITY

Turkish Journal of Nature and Science

e-ISSN: 2149-6366
www.dergipark.gov.tr/tdfd

Research Article

Volume 14, Issue 4, Page 158-164, 2025

Received: 07.07.2025
Accepted: 11.11.2025
Published: 30.12.2025

https://doi.org/10.46810/tdfd.1698919

Synthesis and Characterization of Erbia - Doped Yttria - Stabilized Ceria - Zirconia Based Nanoceramics

Senol DURMUSOGLU[1], Elif Esra ALTUNER[2*]

[1] Kocaeli Health and Technology University, European Vocational school, Hybrid and Energy Department, Hybrid andElectric Vehicles Program, Kocaeli, Turkiye
[2]Kocaeli Health and Technology University, European Vocational school, Medical Services and Techniques Department, Medical Laboratuary Techniques Program, Kocaeli, Turkiye

**Corresponding author: elifesraaltuner@gmail.com*

Abstract

Erbia-doped yttria-stabilized ceria-zirconia-based nanocrystalline ceramics were fabricated via the conversion technique from polymer to ceramic by metal acetate as preceramic hybrid polymer solutions. Samples were characterized by Scanning Electron Microscopy, Fourier Transform Infrared Spectroscopy, and X-ray Diffraction. The nanocrystallite size was evaluated using the Scherrer equation. The crystalline value, which is the lowest, and the crystallite size were determined for the sample comprising Zr (74%), Y (11%), Ce (10%), and Er (5%) in the atomic weight ratio. Scanning Electron Microscopy results indicate that an increase in yttria content increased the agglomeration of the grains. The successful synthesis of mixed oxide structures was validated by FTIR spectra, which also revealed the formation of distinctive metal–oxygen bonds (Zr–O, Ce–O, and Er–O) and the complete breakdown of organic groups. The produced nanoceramics show fine particle shape, homogeneous phase development, and increased structural stability with increasing dopant content, according to the combined FTIR, XRD, and SEM investigations.

Keywords

Nanoceramic, Nanograin, Poly (vinyl alcohol), Yttria, Zirconia

BİNGÖL ÜNİVERSİTESİ

Türk Doğa ve Fen Dergisi

e-ISSN: 2149-6366
www.dergipark.gov.tr/tdfd

Araştırma Makalesi

Cilt 14, Sayı 4, Sayfa 158-164, 2025

Alınış: 07.07.2025
Kabul: 11.11.2025
Basım: 30.12.2025

https://doi.org/10.46810/tdfd.1698919

Erbia - Katkılı İtriya - Stabilizeli Serya - Zirkonyum Bazlı Nanoseramiklerın Sentezi ve Karakterizasyonu

Senol DURMUSOGLU[1], Elif Esra ALTUNER[2*],

[1] Kocaeli Sağlık ve Teknoloji Üniversitesi, Avrupa Meslek Yüksekokulu, Hibrit ve Enerji Bölümü, Hibrid ve Elektrikli Taşıtlar Programı, Kocaeli, Turkiye
[2] Kocaeli Sağlık ve Teknoloji Üniversitesi, Avrupa Meslek Yüksekokulu, Tıbbi Hizmetler ve Teknikler Bölümü, Tıbbi Laboratuvar Teknikleri, Kocaeli, Turkiye

**Sorumlu yazar: elifesraaltuner@gmail.com*

Öz

Erbia- katkılı itriya - stabilizeli seryum-zirkonyum bazlı nanokristalin seramikler, ön seramik hibrit polimer çözeltileri olarak metal asetat ile polimerden seramiğe dönüşüm tekniği ile üretildi. Numuneler Taramalı Elektron Mikroskobu, Fourier Dönüşümlü Kızılötesi Spektroskopisi ve X-ışını Kırınımı ile karakterize edildi. Nanokristalit boyutu Scherrer eşitliği ile değerlendirildi. En az olan kristal değer ve kristalit boyutu, atom ağırlığına oran olarak Zr (%74), Y (%11), Ce (%10) ve Er (%5) içeren numune için elde edildi. Taramalı Elektron Mikroskobu sonuçları itriya içeriğindeki artışın taneciklerin aglomerasyonunu artırdığını göstermektedir. Karışık oksit yapıların başarılı sentezi, belirgin metal-oksijen bağlarının (Zr–O, Ce–O ve Er–O) gelişimini ve organik grupların tamamen parçalanmasını da gösteren FTIR spektrumları ile doğrulandı. Üretilen nanoseramikler, birleşik FTIR, XRD ve SEM incelemelerine göre, ince parçacık şekli, homojen faz gelişimi ve artan katkı maddesi içeriğiyle artan yapısal kararlılık göstermektedir.

Anahtar kelimeler

Nanoseramik,
Nanotanecik,
Poli (vinil alkol),
İtriya,
Zirkonyum

1. INTRODUCTION

Ceria–zirconia (CeO_2–ZrO_2)–based ceramics exhibit high fracture durability and a good oxygen holding/release capacity (OSC)/(ORC). These ceramics are commonly used as a catalyst for preventing sooting in diesel engine exhaust, as an admixture for combustion catalysts, and in fuel cell processes [1-3].

Another significant application of this ceramic is the preparation of surrogate composites to characterize the chemical, physical, and thermal properties of inert matrix fuel (IMF) [4-7].
In this study, CeO_2-ZrO_2-based nanocrystalline ceramics were doped with erbium and yttria to increase the thermal stability of the mixed oxide material [8-10]. Good dispersion and homogenization of mixed oxides are very important key factors in the CeO_2-ZrO_2-based nanostructured ceramics; however, perfect homogenization cannot be easily obtained by the conventional powder mixing and milling fabrication technique [4,5], [8–10].
.
The ceramic powders in this new study were created using the polymer-to-ceramic conversion approach by co-precipitating zirconium, yttrium, and erbium acetate pre-ceramic precursors with the proper amount of poly (vinyl alcohol) (PVA) [4,5,8-12]. Nanostructured materials display outstanding characteristics such as superior stability, strength, and toughness, as is evident from the presence of refined grains [4,11, 14]. The samples are synthesized after mixing and curing stages of the molecular level homogeneously mixed hybrid polymer solution, the removal of the polymeric precursor of PVA, and the conversion of metal acetates to oxide are achieved in the thermal decomposition. The calcination step was achieved with the heat treatment of the polymer solution at 850 °C.

2. EXPERIMENTAL PROCEDURE

Sigma Aldrich provided the zirconium acetate (solution in diluted acetic acid), cerium (III) acetate (Powder), erbium (III) acetate (Powder), yttrium (III) acetate (Powder), and PVA (Powder, Average Mw: 85.000-124.000). Merck supplied the boric acid. The solvent of the solution was ultra-pure deionized water. The experiments comprised three main stages:

Making an initial hybrid polymer (PVA) mixture for the metal acetate composite,

- To create a hydrogel-like solution with metal acetate, the produced polymer solution is warmed in a furnace to 80 °C,
- Calcining or chemically converting the mixture of hydrogel into the wanted nano-scale ceramic powder materials at an increased temperature, with simultaneous drying of all the hybrid PVA polymer solutions from the precursor at 850 °C. The rate of heating and cooling was fixed at 8 °C/min. The PVA solution (10 %) was made up by dissolving the PVA powder into ultrapure deionized water at 80 °C while it was being stirred for 3 hours. The solution was stirred for 2 more hours after it was cooled to room temperature. Then, the solutions of five aqueous metal acetates were separately produced, and 20 g of the aqueous PVA solution (w/w 10 %) was added to these solutions. The values of the metal amounts were given in Table 1 as a percentage of each other.

Table 1. Percentage of metals for the synthetic ceramic materials (wt/wt).

Solution #	Zr%	Y%	Ce%	Er%
IMF-1	88.0	0.0	8.0	4.0
IMF-2	74.0	11.0	10.0	5.0
IMF-3	40.0	42.0	12.0	6.0
IMF-4	19.0	60.0	14.0	7.0
IMF-5	0.0	76.0	16.0	8.0

The final product of the PVA-metal acetate hybrid polymer solutions was a viscosity gel.

After the solutions had evaporated and dried at room temperature, the dried gels were put into ceramic crucibles and calcined for two hours at 850 °C (in an air environment) at a rate of 8 °C per minute. Using a mortar, the oxide ceramic composites that were produced as a result of solutions 1–5, known as IMF 1–5, were crushed into powder. Figure 1 lists the steps of manufacture.

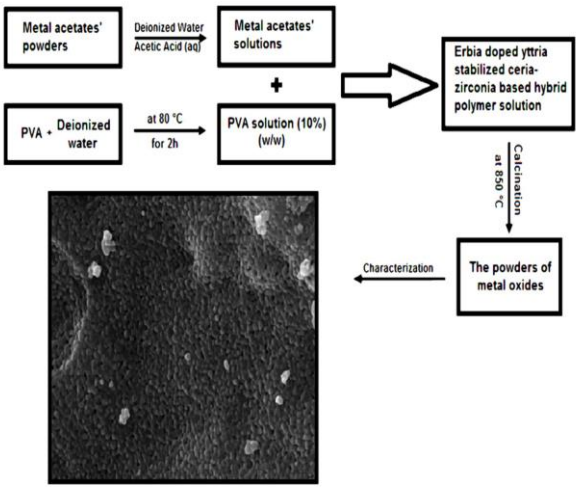

Figure 1. The stages of the production IMF 1-5.

The conductivity and pH values of the solutions were quantified via WissenschaftlichTechnische-Werkstätten WTW and 315i/SET apparatus. The AND SV-10, a viscometer, was used to measure the solutions' viscosity values. The KRUSS tens, a manual measuring tool, was used to quantify the values of surface tension of the mixtures. The measurements of the Fourier Transform Infrared Spectroscopy (with ATR module) results were made via the Thermo Nicolette 6700 spectrophotometer in solutions and nanocomposite powders. The morphology structures of nanocomposites were provided at 10 kV of voltage by Scanning Electron Microscopy via JEOL JSM 6060 on samples with gold sputtering. The diameters of nanoparticles were quantified via ImageJ, associated with image processing software (Image Pro-Express, Version 5.0.1.26, Media Cybernetics Inc., public domain of Java programme). The crystalline structures of

the nanocomposite powders were examined by X-Ray Diffraction via XRD Bruker AXS D8 Advance diffractometer with the Vario1 Johansson focusing monochromator, having Cu Ka1 radiation.

3. RESULTS AND DISCUSSION

The conductivity, pH, surface tension, and viscosity values of the polymer-metal acetates hybrid polymer solutions were quantified, and these figures can be seen in Table 2. According to Table 2, as the contents of cerium, yttrium, and erbium are increased, the conductivity, pH, surface tension, and viscosity values of the solutions increase too.

Table 2. Physical properties of the PVA/Zr-Y-Ce-Er acetate hybrid polymer solution.

Solution #	pH	Viscosity (mPa.s)	Conductivity ($mS.cm^{-1}$)	SurfaceTension ($mN.m^{-1}$)
IMF-1	2.48	28.7	1.535	46
IMF-2	2.64	29.3	1.992	49
IMF-3	2.80	33.7	2.710	51
IMF-4	2.91	35.5	3.200	53
IMF-5	2.95	50.8	3.490	54

To further understand the microstructure of IMF 1-5 solutions and calcined powders, FTIR spectroscopy was used. Figure 2 (a–f) displays the FTIR characterization analysis of the IMF 1–5 solutions and the pure PVA solution. The stretching O-H vibration is linked to the broad bands seen between 3600 and 3200 cm^{-1}, which are brought on by PVA's C=O and C–O stretching, respectively [12, 14]. The O-H vibration is the source of the band seen at 1391 cm^{-1}. The C–O stretching is visible in the band at 1276 cm^{-1} [14]. The characteristic vibration of acetic acid is represented by the band seen at [12, 14]. The band at 1276 cm^{-1} shows the C–O stretching. Acetic acid's typical vibration is indicated by the band visible at 1016 cm^{-1} (CH_3COOH). The out-of-range. Acetic acid's normal vibration is represented by the band seen at 1016 cm^{-1} (CH_3COOH). The out-of-range O-H vibrations in PVA are indicated by the band at 615 cm^{-1} [12-14].

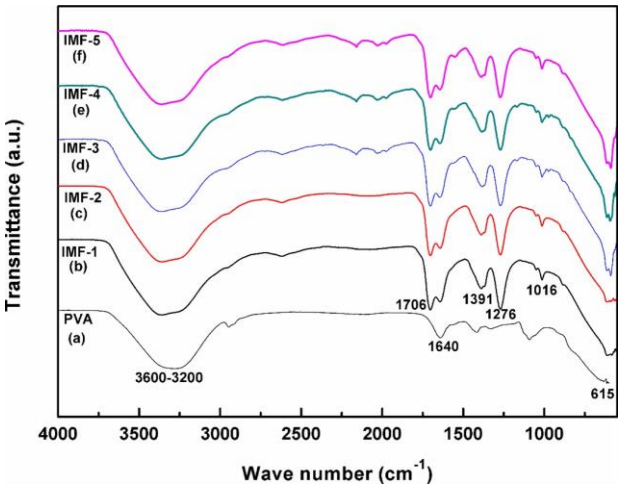

Figure 2. The FTIR spectra of the pure PVA solution (a) and the IMF 1-5 solutions (b-f).

Figure 3 (a-e) is the FTIR spectra of the erbia-doped yttria-stabilized ceria–zirconia nanoceramic samples of powder IMF 1-5. As indicated in the heated IMF 1-5 nanocrystalline powder samples did not display any of the bands at 3000-2840 cm^{-1}, as seen in Figure 3.

Or the bandwidth at 3600-3200 cm^{-1}. As previously mentioned, the stretching C-H and O-H vibrations of the alkyl groups are responsible for these bands, respectively. The lack of these bands indicated that the nanocrystalline powder samples contained neither carbon nor water.

The characteristic bands of yttrium, erbium, cerium, and zirconium oxides are in the fingerprint region. The bands observed at 1558, 1439, 1019, and 941 cm^{-1} are thought to be caused by yttrium, cerium, or erbium oxide. Additionally, the intensity levels of these bands rose as a result of the increase in the amounts of yttrium, cerium, and erbium content.

The calcined nanoceramic particles' FTIR spectra show several distinct absorption bands that are in line with their mixed oxide composition. While small signals around 2920–2850 cm^{-1} are ascribed to C–H stretching from remaining polymer chains, the broad feature between 3600–3200 cm^{-1} corresponds to O–H stretching vibrations of adsorbed hydroxyl groups. Acetate species' C=O stretching is linked to the band at 1635 cm^{-1}, whereas CH_2 scissoring in PVA is the source of the band about 1420 cm^{-1}. The total elimination of organic moieties is confirmed by the loss of C–H and C=O vibrations during calcination. In the meantime, metal–oxygen stretching of Zr–O, Ce–O, and Er–O bonds results in additional absorption peaks between 600 and 500 cm^{-1}, signifying the successful construction of the mixed oxide network. These M-O bands are gradually moving to lower wavenumbers. In the meantime, metal–oxygen stretching of Zr–O, Ce–O, and Er–O bonds results in additional absorption peaks between 600 and 500 cm^{-1}, signifying the successful construction of the mixed oxide network. In good accord with earlier results on rare-earth-doped zirconia systems [12–14], [16–18], a gradual shift of these M–O bands to lower wavenumbers with increasing Er^{3+} and Y^{3+} concentrations suggests stronger metal–oxygen interactions and local lattice distortions.

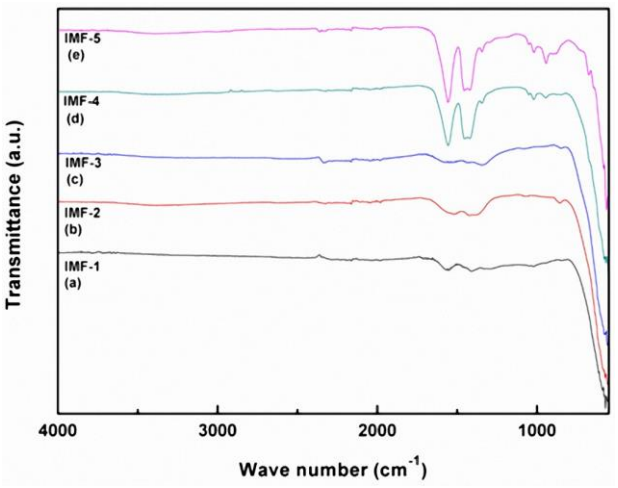

Figure 3. The FTIR results of the erbia doped yttria stabilized ceria – zirconia nanoceramics.

These XRD diffractograms of the erbia-doped yttria-stabilized ceria-zirconia IMF nanopowders are displayed in Figures 4 and 5. In the absence of Y_2O_3, a relatively modest amount of CeO_2 and Er_2O_3 can stabilize the ZrO_2 (for sample IMF-1), according to the X-ray diffraction patterns shown in Figure 4(a). Consequently, a one-phase mixture of stabilized face-centered cubic ZrO_2 structure doped with ceria and erbia was found, exhibiting four reflection peaks at 2θ values and related planes of 29.93° (111), 34.23° (200), 50.10° (220), and 59.75° (311). These peaks align with Figures 4(a,b) and 5(a-c), per JCPDS-International Center for Diffraction Data (PDF # 01-081-1551). As predicted, the ZrO_2 peak intensities declined while the Y_2O_3, CeO_2, and Er_2O_3 peak sizes and intensities grew for the samples IMF-4, IMF-3, and IMF-2 as the cubic structure continued to emerge with enhanced Y_2O_3, CeO_2, and Er_2O_3 content. Face-centered cubic Zr_1-xYxO_2 peaks were seen in the XRD diffractogram at 2θ= 50.18° and 59.40°. These were attributed to the (220), (311) reflection of Zr1-xYxO_2 in the cubic Fm3m phase (JCPDS card # 01-077-2115). Yet, because the IMF-5 sample lacks zirconium, these peaks are not visible. As the CeO_2 concentration increased, robust, face-centered cubic CeA_1-aO_3 peaks emerged at 2θ= 28.89° (222), 33.44° (400), and 48.15° (440). As the cerium concentration increased, the strength of the CeO_2 peaks increased as well, reaching their highest value for the IMF-5 sample. As stated by the JCPDS International Center for Diffraction Data files (JCPDS 01-083-0327), all of the sample peaks may be indexed to a pure body-centered cubic structure of Ce_aY_1-aO_3 (space group: Ia-3). Erbia was dissolved in either zirconia-rich or yttria-rich phases in every sample.

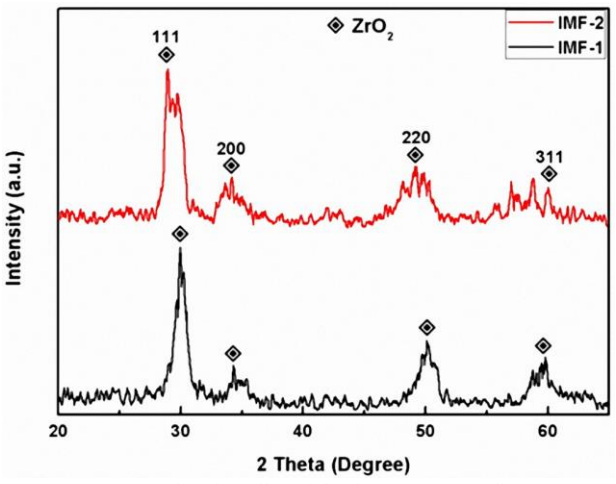

Figure 4. XRD results of small particles for IMF-1 according to IMF-2.

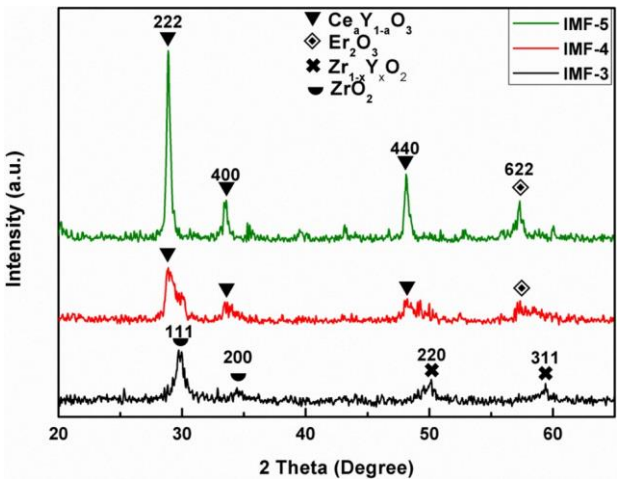

Figure 5. XRD results of sthe particles for , IMF-4, IMF-5, and IMF-3.

The Scherrer equation for equation 1 (Eq.1) was used to determine the crystallite sizes (D) based on the broadening of the (111) and (222) diffraction peaks in the XRD pattern [16-20]:

$$Dhkl = k\lambda / \beta_{hkl} l^{cos\theta} \qquad \text{(Eq.1)} \qquad [15\text{-}20].$$

(Where Dhkl is the mean k = 0.9, λ is the X-ray radiation wavelength (0.15405 nm), θ is the Bragg angle for the crystal planes {hkl}, and βhkl is the peak's broadening (full-width at half-maximum (FWHM)).)

The following relations in equation 2 (Eq.2) were used to compare the peak locations (2^i) of the XRD patterns in order to calculate the lattice characteristics of the composite samples [21].

$$1/d^2 = h^2 + k^2 + l^2/\alpha^2 \qquad \text{(Eq.2)} \quad [20].$$

Table 3 displays the composite samples' calculated structural properties. It is evident from all of the data in Table 3 that our samples lack the tetragonal and monoclinic phases. The IMF-2 sample has the least lattice constant, a, according to the computed findings. For the IMF-2 sample of the (311) reflection, the computed structural lattice parameter, a, was 5.1087 A°.

Figure 6 (a-c) shows SEM results of the Erbia-doped yttria stabilized ceria–zirconia nano-scale crystalline ceramic materials. Only a tiny percentage of the particles exhibit irregular shapes; the majority are spherical in form. Other significant features of the samples derived from SEM analysis include the absence of aggregation and the development of islands of crystal as the samples' yttria concentration rises. Although representative SEM micrographs of the IMF-2–4 samples are presented here, all compositions were synthesized and calcined under identical experimental conditions (10 % PVA, 850 °C, 8 °C min^{-1}). The observed microstructures are therefore consistent across the series, showing similar spherical morphologies and grain coalescence behavior with increasing yttria content. Thus, the displayed SEM images can be regarded as representative for the entire set of nanoceramic samples.

Table 3. Computed the composite samples' structural parameters for each IMF sample.

Sample	(*hkl*)	2θ (°)	*d* (Å)	*a* (Å)	*FWHM* (°)	*D (nm)*
IMF-1	(111)	29.93	2.9829	5.1666	1.0911	7.5364
	(200)	34.23	2.6174	5.2348	-	-
	(220)	50.10	1.8192	5.1456	-	-
	(311)	59.75	1.5464	5.1288	-	-
IMF-2	(111)	29.23	3.0528	5.2875	1.5776	5.2039
	(200)	34.19	2.6204	5.2408	-	-
	(220)	49.37	1.8444	5.2168	-	-
	(311)	60.01	1.5403	5.1087	-	-
IMF-3	(111)	29.75	3.0006	5.1971	0.8161	10.0717
	(200)	34.45	2.6012	5.2024	-	-
	(220)	50.18	1.8165	5.1379	-	-
	(311)	59.40	1.5547	5.1563	-	-
IMF-4	(222)	28.89	3.0879	10.6968	1.3010	6.3055
	(400)	33.44	2.6774	10.7097	-	-
	(440)	48.15	1.8882	10.6816	-	-
	(622)	57.35	1.6053	10.6482	-	-
IMF-5	(222)	28.89	3.0879	10.6968	0.3999	20.5137
	(400)	33.44	2.6774	10.7097	-	-
	(440)	48.15	1.8882	10.6815	-	-
	(622)	57.35	1.6053	10.6482	-	-

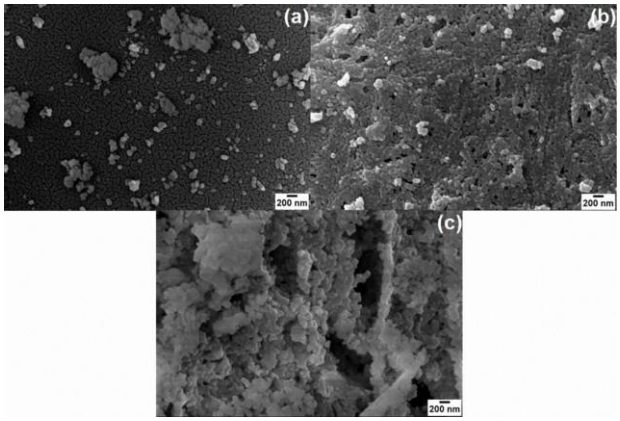

Figure 6. SEM results of the Erbia doped yttria stabilized ceria–zirconia nanocrystalline ceramics using different angles for 200 nm scale (a) IMF-2, (b) IMF-3, and (c) IMF-4.

4. CONCLUSION

In the present study, erbium and yttria-doped CeO_2-ZrO_2 based nanocrystalline ceramics were successfully fabricated using PVA as a polymeric precursor. The obtained nanocrystalline ceramics were characterized by FT-IR, XRD, and SEM techniques. The XRD patterns show cubic ZrO_2, Y_2O_3, Er_2O_3, and CeO_2 crystal materials. SEM characterizations indicate that almost all of the particles are spherical; only a small number of them show an irregular shape. The increase in the amount of Y_2O_3 content in the sample gave rise to an increase in the agglomeration of the grains. Moreover, lattice parameters and crystallite sizes were calculated for all samples. According to calculated results, the smallest lattice constant, a, was obtained for the sample containing Zr (74 %), Y (11 %), Ce (10 %), and Er (5 %) as the ratio of atomic weights. The calculated structural lattice parameter, a, for the sample containing Zr (74 %), Y (11 %), Ce (10 %), and Er (5 %), as the ratio of atomic weight was 5.1087 Å. In addition, the smallest crystallite size, D, was obtained for the sample containing Zr (74 %), Y (11 %), Ce (10 %), and Er (5 %) as the ratio of atomic weights. The calculated crystallite size, D, for the sample containing Zr (74 %), Y (11 %), Ce (10 %), and Er (5 %), as the ratio of atomic weight was 5.2039 nm.

REFERENCES

[1] Bernal S., Kaspar J. , Trovarelli A. Recent Progress in Catalysis by Ceria and Related Compounds, Catal. Today. 1999; 50:173.

[2] Centeno M.A., Paulis M., Montes M., Odriozola J.A. Catalytic combustion of volatile organic compounds on $Au/CeO_2/Al_2O_3$ and Au/Al_2O_3 catalysts, Appl. Catal. A-Gen. 2002; 234(1-2):65-67.

[3] Shan W., Liu F., Yu Y., He H. The use of ceria for the selective catalytic reduction of NOx with NH_3, Chineese Journal of Catalysis. 20014; 35(8): 1251-1259.

[4] Grover V., Tyagi A.K. Investigations of Ternary Phase Relations in a CeO_2–Gd_2O_3–ThO_2 System, *J. Am. Ceram. Soc.* 2006; 89(9):2917-2921.

[5] Somers J., Papaioannou, D., McGinley J., Sommer, J. Safety assessment of plutonium mixed oxide fuel irradiated up to 37.7 GW day tonne^{-1}, Journal of Nuclear Materials. 2013;437(1-3):303-309.

[6] Suda A., Yamamura K., Morikawa A.,Nagai Y., Sobukawa Y., Ukyo Y., et al. Atmospheric pressure solvothermal synthesis of ceria–zirconia solid solutions and their large oxygen storage capacity, Journal of Materials Sciences, 2008; 43: 2258–2262..

[7] Uslu I., Aytimur A., Ozturk M.K., Kocyigit S. Synthesis and characterization of neodymium doped ceria nanocrystalline ceramic structures, Ceram. Int., 2012; 38(6): 4943-4951.

[8] Chavan S.V., Mathews M.D., Tyagi A.K. Phase relations and thermal expansion studies in the CeO_2–$NdO_{1.5}$ system, Materials Research Bulletin. 2005; 40(9): 1558-1568.

[9] Degueldre C., Paratte J.M. Concepts for an inert matrix fuel, an overview, J. Nucl. Mater. 1999; 274;(1-2):1-6.

[10] Stan M., Armstrong T.J., Butt D.P., Wallace T.C., Park Y.S., Haertling C.L., Hartmann T., Hanrahan R.J., Stability of the Perovskite Compounds in the Ce-Ga-O and Pu-Ga-O Systems, *J. Am. Ceram. Soc*. 2002; 85(11):2811-2816.

[11] Chandramouli V., Anthonysamy S., Rao P.R.V., Combustion synthesis of thoria – a feasibility study, J. Nucl. Mater. 1999; 265:255-261.
[12] Uslu I., Aytimur A., Production and characterization of poly(vinyl alcohol)/poly(vinylpyrrolidone) iodine/poly(ethylene glycol) electrospun fibers with (hydroxypropyl)methyl cellulose and aloe vera as promising material for wound dressing, J. *Appl. Polym. Sci.* 2012; 124(4):3520-3524.
[13] Andrade G., . Barbosa-Stancioli E.F, Mansur A.A.P., Vasconcelos W.L., Mansur H.S. Design of novel hybrid organic-inorganic nanostructured biomaterials for immunoassay applications, Biomed. Mater. 2006;1(4):221-34.
[14] Aytimur A., Uslu I., Kocyigit S., Ozcan F. Magnesia stabilized zirconia doped with boron, ceria and gadolinia Ceram. Int. 2012; 38: 3851.
[15] Alvarado E., Torres-Martinez L.M., Fuentes A.F., Quintana P., Preparation and characterization of MgO powders obtained from different magnesium salts and the mineral dolomite, Polyhedron 2000; 19(22-23): 2345-2351.
[16] Ding Y., Zhang G.T., Wu H., Hai B., Wang L.B., Qian Y.T., Nanoscale Magnesium Hydroxide and Magnesium Oxide Powders: Control over Size, Shape, and Structure via Hydrothermal Synthesis, *Chem. Mater.* 2001; 13(2): 435.
[17] Karunagaran B., Kumar R.T.R., Mangalaraj D., Narayandass S.K., Rao G.M., Influence of thermal annealing on the composition and structural parameters of DC magnetron sputtered titanium dioxide thin films, Cryst. Res. Technol. 2002(37):1285.
[18] Klug P.H., Alexander L.E., X-ray Diffraction Procedures for Polycrystalline and Amorphous Materials, John Wiley & Sons, New York, 1974(1).
[19] Prasad N., Varma, K.B.R. Nanocrystallization of $SrBi_2Nb_2O_9$ from glasses in the system $Li_2B_4O_7$ SrO Bi_2O_3 Nb_2O_5, *Mater. Sci. Eng. B-Adv.* 2002; 90(3): 246-253.
[20] Suryanarayana C., Norton M.G., X-ray diffraction a practical approach, X-ray Diffraction. Plenum Press, New York, 1998; 1:3-19.
[21] Vishunumurthy G., Bhaskar A., A Comprehensive Study on the Impact of Aluminum Doping on X-ray Diffraction Peak Profile Analysis, Structural, Morphological, and Optical Properties of ZnO Nanoparticles Synthesized by Sol–Gel Auto-Combustion, Journal of Electronic Materials. 2025; 54: 2146–2166.
[22] Çılğın E. Synergistic effects of SWCNT and MgO nanoparticle additives on engine performance and emissions: a laboratory analysis approach, Biofuels. 2025; 1759-7277.
[23] Kaya, N. Analysis of the physical properties of MgB_2 superconductor with $Zn(NO_3)_2{\cdot}6H_2O$, Journal of Materials Science: Materials in Electronics. 2025; 36(5).